FAINT STREAK DETECTION WITH CERTIFICATE BY ADAPTIVE MULTI-LEVEL BAYESIAN INFERENCE

Radim Sara and Vojtech Cvrcek

Department of Cybernetics, Czech Technical University in Prague, Czech Republic
Email: {sara,cvrcevo1}@cmp.felk.cvut.cz

ABSTRACT

It is known that detecting straight streaks from fast moving celestial objects in optical images is an easy problem as long as the streaks are sufficiently long and/or their signal-to-background (SBR) is sufficiently high.

At low SBR the situation is different. Since the SBR can be arbitrarily small in practice, a good detection procedure has to provide a detection certificate which is a yes/no answer to the question "does the image contain a streak?" In this paper we pose detection with certificate as a Multi-Level Bayesian Inference (MLBI) problem which is based on Bayesian model selection. We describe the algorithm and show an experimental proof of good behavior on synthetic streaks over real image data.

A systematic performance evaluation shows that MLBI confirms and partially exceeds results of state-of-the art methods. In particular, in the class of difficult problem instances with SBR of $0\,\mathrm{dB}$ to $-5\,\mathrm{dB}$ and streak length 10 to 500 pixels, we achieved $\mathrm{AUC} \approx 0.97$, which means that the Bayesian detection certificate is wrong in just 3% of cases.

Keywords: streak detection; detection certificate; Bayesian inference.

1. INTRODUCTION

We consider the problem of detecting faint straight streaks created by fast moving celestial objects in images from an optical telescope. For the purpose of this paper a streak is a line segment of unknown position, length, orientation, and amplitude (magnitude). An example is shown in Fig. 1. The task of streak detection is two-fold: (1) decision on whether a given image contains a streak, and (2) determining the four principal parameters of the streak (orientation, starting position, length).

It is known that detecting such streaks is an easy problem as long as the streaks are sufficiently long and/or their signal-to-background ratio (SBR) is sufficiently high, eg. [16, 19, 12].

Several detection methods have been proposed in the past. In a segmentation based approach [6], authors use a threshold to segment image to objects of interest and a background. The objects are characterized by their shape and located in other images. The method is therefore capable of object tracking across several images. The work [6] is the oldest method we are aware of. A recent method called Line-Identifying Technique [9] bears some similarities. These methods are suitable for fast detection of short streaks with a high SBR. More advanced methods that allow tracking of streak across several images include the stacking method [17] and a particle based tracking [13]. While it is desirable from the detection point of view to use multiple images to obtain as much information about the streaking object as possible, such approach is not applicable to cases of a fast moving object that is observed just once. Such objects are in focus of the current paper.

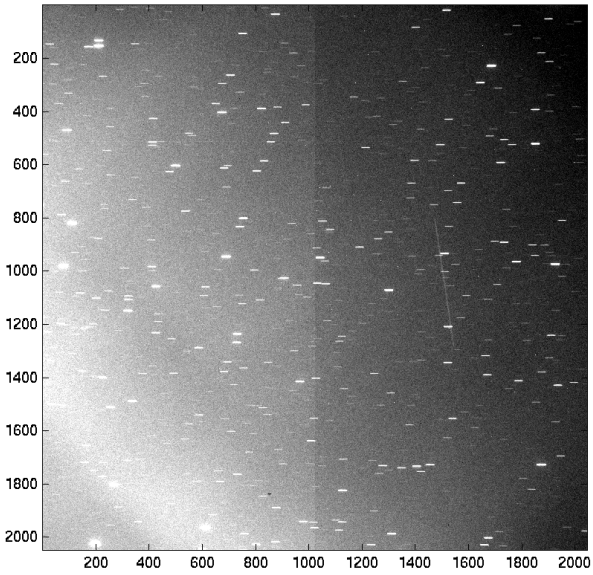

Figure 1. A well-detectable streak (about 500 px long and almost vertical in the middle of the right (darker) part of the field of view). Best viewed on a good monitor.

The method [12] uses image transformation (skewing, compression) to increase SBR in a single image to obtain an initial detection. The method then tracks streaks in subsequent images by assuming linear motion of the

streaks and correlating the streak candidates.

Lastly, there are methods that detect streak in a single image. Radon/Hough transformation based method [19, 1] are used. The advantage of these methods is that they are easily parallelized [19]. Such methods allow to select quantization in Radon/Hough space. The quantization chooses a trade-off between accuracy and speed. We also saw use of matched filters [4, 11]. Such methods use a large variety of filters, each filter representing a different shape of a streak.

The Line Detection Method [16] removes stars from a raw image, tries all rotations of the image and computes columnwise medians in rotated images. A tentative streak is then located in the column of the largest median, one tentative streak per rotation angle. The algorithm then outputs the tentative streak of the largest columnwise response. Later, [12] proposed image shearing instead of rotation because it is faster to compute.

The median computation can be perceived as the simplest statistical method for streak detection. In the current paper we borrow the idea of image shearing and tentative streak detection per shear angle. Instead of image shearing with fine angular increments we use an efficient branch-and-bound approach.

The method [5] develops a full statistical model for the streak (background, stars) and determines the most likely hypotheses (streak, background, star). This method is closest to our approach from the statistical modeling point of view.

A complete pipeline developed in ESA-funded StreakDet project is described in [14]. They achieved fast processing time with an image preprocessing method that is essentially a set of grayscale and binary morphological operations followed by connected component labeling. They report detection sensitivity 90% for $\mathrm{SNR} > 1$ and 50% for $\mathrm{SNR} = 0.5$ at streak length of $100\,\mathrm{px}$ and longer.

At low signal-to-background ratio (SBR) it becomes difficult to decide on a streak presence in the image for two principal reasons: (1) as the SBR limits to zero the statistical characteristics of a streak become indistinguishable from those of the background, partly due to the finite resolution of the sensor (its limiting magnitude), (2) as the streak gets shorter then it is progressively more difficult to distinguish it from a random configuration of image background that falsely resembles a streak. A good detection procedure thus has to provide a "detection certificate" which is a yes/no answer to the question "does the image contain a streak?" The difficulty of this task stems partly from the fact that any kind of a "decision threshold" depends on streak length, image content, SBR, and sensor characteristics, so it cannot be chosen apriori.

A statistical detection procedure that works step-wise would first detect a candidate streak and then use a statistical test on the rest of the image to see how likely it is that a similar configuration does not appear by chance. In this paper we formulate the detection as Multi-Level Bayesian Inference Problem (MLBI) [8] that works in an opposite fashion: It confirms/disproves a streak presence in the image and locates it afterwards. We develop two probabilistic models describing a given image: (1) the image contains no streak, and (2) the image contains a single streak. Decision on streak presence is then a decision on which model is explaining the image better. The quality of a model is evaluated by its *Bayesian evidence*. We show that computing the Bayesian evidence in our model is possible with a fast polynomial algorithm. The method will be described in Sec. 2.5.

Algorithm 1 (Distribution Parameter Learning)**.**
For a given image shear angle ϕ:

1. *Represent image by steerable filter similarity map $X = \{x_{i,j}\}$.*
2. *Learn pixelwise background distribution parameters θ in $p_b(x_{i,j} \mid \phi_l; \theta)$.*
3. *Compute pixelwise streak model in $p_s(x_{i,j} \mid \phi_l; \theta)$ by distribution composition.*

Figure 2. A sketch of the image preprocessing procedure.

2. METHOD

As a guidance to the reader, we sketch our preprocessing in Fig. 2 and the actual multi-level Bayesian inference in Fig. 5. These are not self-explanatory without reading this section.

2.1. Image Representation

We use an image model of a streak segment in the form of an image filter. The filter works like a convolution kernel in the same sense as a matched filter. The important difference is that we do not model the entire streak, just its short segment (eg. 51 pixels). Normalized correlation of the image and the filter limits the influence of the image brightness and contrast variations on detection. Such contrast-enhancing technique is a well-known practice. Since the template is oriented, we need to evaluate the filter responses for all possible image shearing angles. Instead of filtering the image per shearing angle we represent the image by a bank of steerable filters whose response at a given angle can be computed locally and very fast without repeating the image correlations.

We use spherical quadrature filters (SQF) [3] and the feature vector for the local signal representation [10]. Instead of measuring feature vector distance as in [10], we use similarity based on the dot product. Let $\mathbf{t} = (t^1, t^2, \ldots, t^n) \in \mathbb{C}^n$ be the template complex vector for line segment signal type, this is $\mathbf{t}_L$ from [10], where n is the largest order of the generalized Hilbert transform kernel (see also [15]). We exclude the input signal itself because we need invariance to additive constant function. Let $\mathbf{f} = (f^1, f^2, \ldots, f^n) \in \mathbb{C}^n$ be the image feature vector computed in a pixel as a set of responses to the SQF.

Then the normalized similarity of local image neighborhood to template $\mathbf{t}$ at orientation angle ϕ is

$$x_\phi(\mathbf{f}, \mathbf{t}) = \left\langle \frac{\mathbf{f}}{\|\mathbf{f}\|}, \mathbf{r}(\phi) \odot \frac{\mathbf{t}}{\|\mathbf{t}\|} \right\rangle, \tag{1}$$

where $\langle \mathbf{a}, \mathbf{b} \rangle$ is the complex dot-product,

$$\mathbf{r}(\phi) = (r^1(\phi), \ldots, r^n(\phi)), \quad r^k(\phi) = e^{ik\phi}, \; k \in \mathbb{N}^n$$

is a rotation vector, and $\odot$ is the elementwise (Hadamard) product. We used $n = 8$ but took only the four even filters. Computing (1) for a given angle ϕ is much faster than computing the full template correlation per ϕ from scratch.

For the sake of columnwise streak detection described later in this section it is still necessary to perform image shearing. Instead of shearing the raw image, we shear the similarity image. We thus do not save time on shearing but do avoid the time needed for computing very many repeated template correlations per angle.

2.2. A Streakless Image Model

Our probabilistic model assumes the existence of a joint probability distribution for a streakless image. Let $\mathcal{X}_\phi$ be the domain of an image sheared by ϕ. Let $x_{\phi,i,j}$ be the oriented filter response from (1) at pixel $(i, j) \in \mathcal{X}_\phi$, and $X_\phi = \{x_{\phi,1,1}, x_{\phi,1,2}, \ldots.\}$ be the entire response field over $\mathcal{X}_\phi$ which we call the streak similarity image (per shearing angle). We assume there is a probability density

$$p_b(X_\phi \mid \phi; \theta(\phi)) = \prod_{i,j \in \mathcal{X}_\phi} p_b(x_{\phi,i,j} \mid \phi; \theta(\phi))$$

per angle ϕ, with parameters $\theta(\phi)$ learned from the similarity image. To unclutter the mathematical expressions, we simplify the notation to

$$p_b(X \mid \phi; \theta) = \prod_{i,j \in \mathcal{X}} p_b(x_{i,j} \mid \phi; \theta), \tag{2}$$

being aware of the fact that $\mathcal{X}$, X and θ are in fact dependent on ϕ.

We need to learn θ from the similarity image. This is done by assuming that $p_b(x_{i,j} \mid \phi; \theta)$ is well-approximated with a two-component mixture of beta distributions and using the EM algorithm for learning the five parameters of this mixture. A typical fit shown over the histogram of X is shown in Fig. 3. In case the input image does contain a streak, we ignore it when learning θ. Its influence on the distribution is very low and can be neglected, as long as the image is large enough. Hence, we call (2) the *background model*. Its pixelwise independence assumption is realistic as long as the diameter of the stars in the image is comparable to pixel size.

2.3. A Single Streak Image Model

We also need to develop a probabilistic model for an image with a streak. We assume the domain of the streak is a subset of pixels $\mathcal{Y} \subset \mathcal{X}$. The shape of the set $\mathcal{Y}$ is modeled implicitly by assuming there is an image shearing angle ϕ that makes the streak located in column j, starting at position i_1 and ending at i_2 in the sheared image.

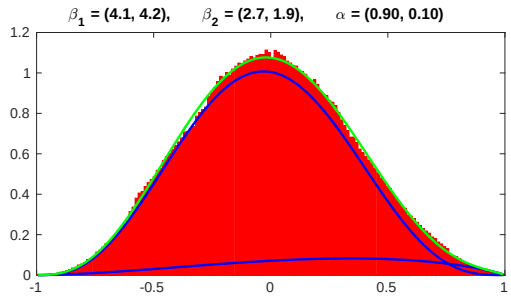

Figure 3. A typical background model fit (green) over the histogram of oriented filter responses for a given image and angle $\phi = 30°$.

We do not know the magnitude of the streak and we do not want to model it. We therefore derive a composed model. Consider a single component of a beta distribution mixture over the interval $x \in [-1, 1]$:

$$p(x; a, b) = \frac{1}{2B(a, b)} \left(\frac{1+x}{2}\right)^{a-1} \left(\frac{1-x}{2}\right)^{b-1}. \tag{3}$$

We introduce an auxiliary parameter $z \in [0, 1]$ such that

$$a = \alpha + z\beta, \quad b = (1 - \beta)z + \beta.$$

This defines a family of densities $p(x \mid z; \alpha, \beta)$. The z 'steers' the density so that $z = 0$ corresponds to the background mixture component with parameters α, β and $z = 1$ corresponds to a beta p.d.f. with a single parameter and mode at $x = 1$. Indirectly, the z parameter corresponds to streak amplitude. Since we do not know the amplitude we assume the existence of a density $p(z)$ and create a compound density for a streak pixel filter response

$$p_s(x_{i,j} \mid \phi; \theta) = \int_0^1 p(x_{i,j} \mid \phi, z; \alpha, \beta)\, p(z)\, \mathrm{d}z, \tag{4}$$

where $\theta = (\alpha, \beta)$. We use uniform $p(z)$ and perform the integration numerically. This is done only once per angle ϕ and per component in the beta mixture. The final density is defined by mixing the compound components (4) with the original mixing parameters. The shape of a compound distribution for a single beta p.d.f. is shown in Fig. 4.

If Y are the filter responses over the set of streak pixels $\mathcal{Y}$ then the p.d.f. of an image with a streak is

$$p_s(X \mid \phi, \mathcal{Y}; \theta) = \prod_{(i,j) \in \mathcal{Y}} p_s(x_{i,j} \mid \phi; \theta) \prod_{(i,j) \in \mathcal{X} \setminus \mathcal{Y}} p_b(x_{i,j} \mid \phi; \theta), \tag{5}$$

where we lumped the parameters of the background model, including the mixing parameters, in $\theta = \theta(\phi)$.

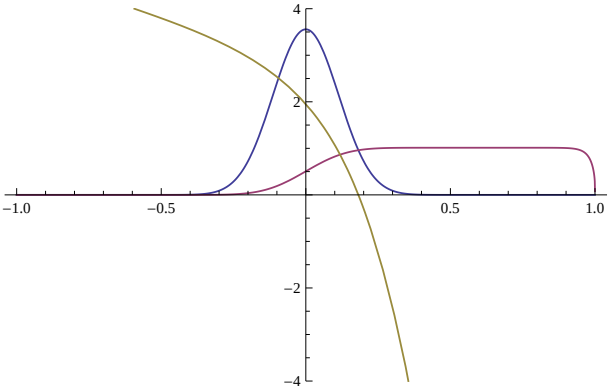

Figure 4. Distribution (3) *(blue) and* (4) *(dark red) and the logarithm of their ratio (dark green).*

2.4. The Full Bayesian Model

The data term of the probabilistic model that will be used for the streak detection consists of (2) and (5) whose parameters θ are shared. For the Bayesian inference (streak detection) we need full models that involve parameters defining streak position $\mathcal{Y}$ in the image.

For the streakless model we simply use

$$p_0(X, \phi;\, \theta) = p_b(X \mid \phi;\, \theta)\, p(\phi). \tag{6}$$

As for the single streak model, we parameterize $\mathcal{Y}$ by column j in the sheared image, and by starting and ending rows in the sheared image, i_1, i_2, respectively. We then define

$$\begin{aligned} &p_1(X, \phi, j, i_{1,2};\, \theta) = \\ &\quad p_s(X \mid \phi, j, i_{1,2};\, \theta)\, p(i_{1,2} \mid \phi, j)\, p(j \mid \phi)\, p(\phi), \end{aligned} \tag{7}$$

where $p(\phi)$ is the same as in (6). Notationally, $\mathcal{Y}$ is now represented by (j, i_1, i_2), so, formally, $p_s(X \mid \phi, j, i_{1,2};\, \theta)$ is equivalent to $p_s(X \mid \phi, \mathcal{Y};\, \theta)$ from (5).

The choice for $p(i_{1,2} \mid \phi, j)$, $p(j \mid \phi)$, and $p(\phi)$ is discussed in Sec. 2.8.

Note again that we learn a pair of distributions $p_0(\cdot)$ and $p_1(\cdot)$ for each image and for each shearing angle ϕ. This gives the method a certain degree of adaptivity to the properties of the current image.

2.5. Multi-Level Bayesian Inference

In this section we drop the parameters θ from the formulas. These parameters are considered fixed (learned, as described in Sec. 2.3).

The Bayesian model selection works by choosing the single-streak model over the streakless model when

$$p_1(X) > p_0(X), \tag{8}$$

Algorithm 2 (MLBI)**.**

1. *For a controlled set of angles ϕ_l do:*
   (a) *shear image by ϕ_l,*
   (b) *learn parameters by Alg. 1,*
   (c) *compute $p_0(X \mid \phi_l)$ from* (17)*,*
   (d) *for all columns j compute and remember,*
      i. *R_{j,ϕ_l} from* (28)*,*
      ii. $i^l_{1,2} \leftarrow \operatorname{argmax}_{i_{1,2}} p_1(X, i_{1,2} \mid \phi_l, j)$,
   (e) $p_0(X \mid \phi_l) \leftarrow \prod_{k=1}^{n_l} p_0(X \mid \phi_l, j)$,
   (f) $p_1(X, j \mid \phi_l) \leftarrow p_0(X \mid \phi_l)\, R_{j,\phi_l}$,
   (g) $p_1(X \mid \phi_l) \leftarrow \sum_{j=1}^{n_l} p_1(X, j \mid \phi_l)$,
2. *compute $p_1(X)$ by integrating $p_1(X \mid \phi_l)\, p(\phi_l)$,*
3. *compute $p_0(X)$ by integrating $p_0(X \mid \phi_l)\, p(\phi_l)$,*
4. *if $p_1(X)/p_0(X) < T$ then output certificate $c \leftarrow 0$ and exit*
5. *else output certificate $c \leftarrow 1$ and streak detection*

$$\begin{aligned} \phi^* &\leftarrow \operatorname*{argmax}_l p_1(X, \phi_l), \\ j^* &\leftarrow \operatorname*{argmax}_j p_1(X, j \mid \phi^*), \\ i^*_{1,2} &\leftarrow \operatorname*{argmax}_{i_{1,2}} p_1(X, i_{1,2} \mid \phi^*, j^*). \end{aligned}$$

Figure 5. A sketch of the proposed certification snd detection procedure.

in which $p_{0,1}(X)$ are the marginals of the distributions (6) and (7), respectively. They are

$$\begin{aligned} p_1(X) &= \int_0^\pi \sum_{j=1}^{n_\phi} \sum_{i_1=1}^{m_\phi} \sum_{i_2=i_1+1}^{m_\phi} p_1(X, \phi, j, i_{1,2})\, \mathrm{d}\phi, \\ p_0(X) &= \int_0^\pi p_0(X, \phi)\, \mathrm{d}\phi. \end{aligned} \tag{9}$$

On the other hand, the parameters of the detected streak are typically obtained by solving a maximization problem

$$\operatorname*{argmax}_{\phi, j, i_{1,2}} p_1(X, \phi, j, i_{1,2}). \tag{10}$$

The computation for $p_1(X)$ must follow a hierarchical scheme: (1) compute columnwise partial sums, (3) sum the columnwise sums over all columns and (3) integrate the result over all angles ϕ. The hierarchy calls for the following inference scheme, which we call Multi-Level Bayesian Inference:

1. If

$$\frac{p_1(X)}{p_0(X)} > T, \tag{11}$$

then the streak presence certificate is $c^* = 1$, otherwise it is $c^* = 0$.

2. If $c^* = 0$ then stop. There is no streak in the image.

3. Decide the orientation of the streak by solving

$$\phi^* = \operatorname*{argmax}_{\phi} p_1(X, \phi), \tag{12}$$

in which $p_1(X, \phi)$ is the marginal of $p_1(X, \phi, j, i_{1,2})$.

4. Assuming the streak angle is ϕ^*, decide the column in which the streak is located by solving

$$j^* = \operatorname*{argmax}_{j} p_1(X, j \mid \phi^*), \tag{13}$$

in which we work with the marginal of $p_1(X, j, i_{1,2} \mid \phi^*)$.

5. Assuming ϕ^* and j^*, determine the streak starting and ending pixel by solving

$$i^*_{1,2} = \operatorname*{argmax}_{i_{1,2}} p_1(X, i_{1,2} \mid \phi^*, j^*). \tag{14}$$

The evidence threshold T for a positive certificate in (11) can be thought of as the ratio of streak occurrence priors

$$T = \frac{1 - P_1}{P_1}, \tag{15}$$

where P_1 is the apriori probability that a random image contains a streak. Typically $T \gg 1$. In practice, the T allows us control the false positive/false negative tradeoff. Details and discussion are given in Secs. 3 and 4.

The actual computation uses the fact that the we can conveniently write

$$\frac{p_s(X \mid \phi, j, i_{1,2})}{p_0(X \mid \phi)} = \prod_{i=i_1}^{i_2} \frac{p_s(x_{i,j} \mid \phi)}{p_b(x_{i,j} \mid \phi)} \tag{16}$$

and

$$p_0(X \mid \phi) = \prod_{k=1}^{m_\phi} \prod_{l=1}^{n_\phi} p_b(x_{k,l} \mid \phi), \tag{17}$$

where $m_\phi \times n_\phi$ is the sheared similarity image size.

Since the evidence of the streakless model does not require summing over streak positions, we can directly use (17). After integrating over all shear angles, we get:

$$p_0(X) = \int_\Phi p_0(X \mid \phi)\, p(\phi)\, \mathrm{d}\phi, \tag{18}$$

where the domain Φ is discussed in detail in Sec. 2.8.

Going bottom up, the (14) is the standard detection by maximization. We have to solve one such task per angle ϕ and column j. It is only necessary to remember the best solution.

By summing over all possible streak begin points and endpoints for each column j given angle ϕ, we have

$$p_1(X, j \mid \phi) = \sum_{i_{1,2}} p_s(X \mid j, \phi, i_{1,2})\, p(i_{1,2} \mid \phi, j)\, p(j \mid \phi). \tag{19}$$

Sec. 2.6 discusses an algorithm for computing (19) efficiently.

By summing over all possible columns, we obtain

$$p_1(X, \phi) = \sum_j p_1(X, j \mid \phi)\, p(\phi). \tag{20}$$

At the top level we integrate over all admissible angles Φ and obtain

$$p_1(X) = \int_\Phi p_1(X, \phi)\, \mathrm{d}\phi. \tag{21}$$

2.6. Efficient Computation of Column Evidence

We can efficiently (in $\mathcal{O}(m_{j,\phi})$) compute the column evidence $p_1(X, j \mid \phi)$. The algorithm is an application of the dynamic programming principle.

Instead of computing $p_1(X, j \mid \phi)$, we compute evidence ratio

$$R_{j,\phi} = \frac{p_1(X, j \mid \phi)}{p_0(X \mid \phi)}. \tag{22}$$

We assume uniformity $p(i_{1,2} \mid \phi, j) = h(m_{j,\phi})$, where $m_{j,\phi}$ depends on the varying number of valid pixels in a sheared image column j and substitute (16) and (17) into (22)

$$R_{j,\phi} = h(m_{j,\phi})\, p(j \mid \phi) \sum_{i_{1,2}} \prod_{i=i_1}^{i_2} \frac{p_s(x_{i,j}|\phi)}{p_b(x_{i,j}|\phi)}. \tag{23}$$

We introduce a new variable

$$V_k = \log \frac{p_s(x_{k,j} \mid \phi)}{p_b(x_{k,j} \mid \phi)}. \tag{24}$$

The logarithm provides numerical stability. Then

$$R_{j,\phi} = h(m_{j,\phi})\, p(j \mid \phi) \sum_{i_{1,2}} \exp\Big[\sum_{i=i_1}^{i_2} V_i\Big]. \tag{25}$$

When we use

$$g(i_1, i_2) = \exp\Big[\sum_{i=i_1}^{i_2} V_i\Big], \tag{26}$$

$$f(i) = \sum_{i_1, i_2 \le i} g(i_1, i_2), \tag{27}$$

then (25) becomes

$$R_{j,\phi} = h(m_{j,\phi})\, p(j \mid \phi)\, f(m_{j,\phi}). \tag{28}$$

There is a recurrent formula for (27) and $k = 1, \ldots, m_{j,\phi}$

$$f(k) = f(k-1) + \sum_{l=1}^{k} g(l,k) = f(k-1) + d(k), \quad (29)$$

with $f(0) = 0$. Lastly, there is a recurrent formula

$$d(k) = \sum_{l=1}^{k} g(l,k) = (d(k-1)+1)\exp(V_k), \quad (30)$$

with $d(0) = 0$.

2.7. Computing Certificate Evidence

Another difficult part is computing the integrals

$$p_i(X) = \int_{\Phi} p_i(X,\phi)\,\mathrm{d}\phi, \quad i = 0, 1.$$

We need to perform the integration numerically with the resolution of the admissible shearing angle set Φ fine enough so that we can capture streaks that manifest themselves as a very sharp peaks of the function $p_1(X,\phi)$. Part of the problem is that the peaks are easily too large for the double float numerical type. We therefore use trapezoidal integration rule with variable precision arithmetic. The integration is done only once per image, hence the computation is not a speed bottleneck.

The set of angles ϕ_k needed in the trapezoidal integration is obtained by a branch-and-bound kind of a procedure:

1. The set Φ is first sampled at a coarse angular resolution (with five-degree angular increments). This gives the initial pool $P = \{\phi_k\}$.
2. All local maxima $\phi_k \in P$ with $|\phi_{k+1} - \phi_{k-1}| > \delta_\phi$ and such that they are larger than a threshold

   $$p(X,\phi_k) > \varepsilon \max_{\phi \in P} p(X,\phi)$$

   expand the pool by adding ϕ_+ to P such that

   $$\phi_+ = \begin{cases} \frac{1}{2}(\phi_{k-1} + \phi_k), & |\phi_k - \phi_{k-1}| > |\phi_{k+1} - \phi_k|, \\ \frac{1}{2}(\phi_k + \phi_{k+1}), & \text{otherwise} \end{cases} \quad (31)$$

3. Step 2 is repeated until there is no expandable ϕ_k.

We use $\delta_\phi = 1/m$ (in radians) where m is the number of image rows and $\varepsilon = 0.3$. The pool P is also used for the streak detection problem (13) and (14). A discussion on the assumptions that make this procedure correct can be found in [7]. The algorithm relies on a property of $p(X,\phi)$: It must make a significant increase in a coarse vicinity of its local maxima caused by streaks. This is true, since if the angle ϕ gets close to the streak orientation angle, the SQF streak segment filter response becomes already large due to its non-zero width and short length. See Fig. 6. The coarse angular resolution in Step 1 of the above procedure is therefore given by the shape of the SQF filter.

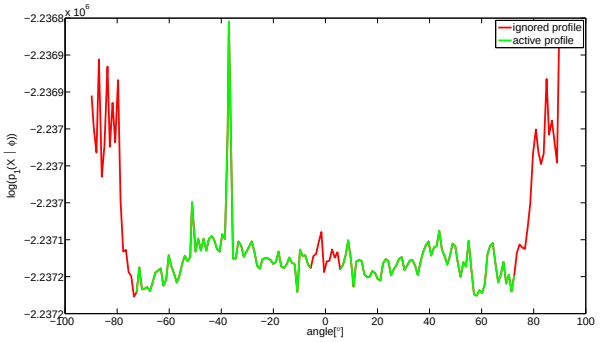

Figure 6. The angular profile $p_1(X \mid \phi)$ of a streak image (from Fig. 10). The green line is the part of the profile we work with (e.g. integrate over). The red line is the part of the profile outside of Φ. The peak close to the angular value of $-40°$ is induced by the streak.

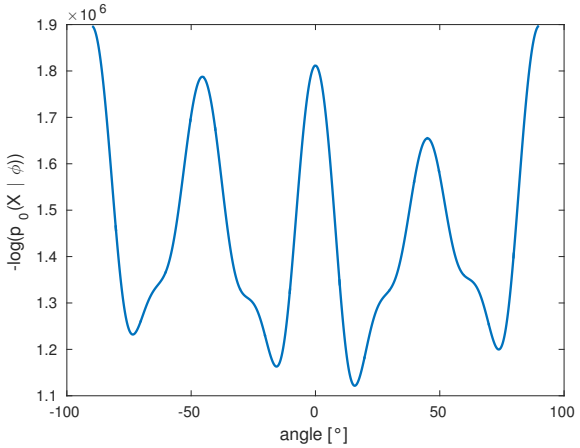

Figure 7. Filter sensitivity for different angles (background image).

2.8. Priors

We chose a uniform distribution

$$p(i_{1,2} \mid \phi, j) = \binom{m_{j,\phi}}{2}^{-1}$$

which takes into account the varying number of valid pixels in a sheared image column j. We also use uniform

$$p(j \mid \phi) = {n_\phi}^{-1},$$

where n_ϕ is the number of columns in image sheared by angle ϕ.

We observed that the streakless model evidence $p_0(X \mid \phi)$ is heavily dependent on ϕ, a typical situation is shown in Fig. 7. The largest deviations occur around angles $\phi = 0°$ $\phi = \pm 45°$, and $\phi = \pm 90°$. We observed that this artefact is partially caused by non-zero contrast between the CCD chip segments (visible in Fig. 1). Sometimes, the boundary is even falsely detected as a streak. Another factor influencing this artefact is the discreteness of the

SQF filter kernels that are not completely rotationally covariant as they should be.

In this paper we mitigated the artefacts by using $p(\phi)$ as a counter-weight. We fit $p(\phi)$ to each image such that

$$p_0(X \mid \phi)\, p(\phi) = \kappa(X), \tag{32}$$

where $\kappa(X)$ is a constant per image X. We essentially learn the prior distribution for shearing angles

$$p(\phi) \propto \begin{cases} 0, & \phi \notin \Phi, \\ \frac{1}{p_0(X|\phi)}, & \phi \in \Phi, \end{cases} \tag{33}$$

where the $p(\phi)$ is obtained after renormalization. We use interval $\Phi = [-73.5, -5.5] \cup [5.5, 73.5]$ as a way to reduce the effect of CCD chip structure.

This procedure could be viewed as a way of learning a background evidence independent on the shear angle, i.e. $p_0(X \mid \phi) = p_0(X)$. This is quite a strong assumption: A complete removal of angular anisotropy is a good model only if the images are obtained by a telescope with sidereal tracking so that stars do not appear as short streaks. Otherwise, it must be taken into account that finding a streak parallel to the stars streaks is a more difficult problem than finding a streak at a different orientation. From a theoretical point of view, this should pose no problem to the MLBI. Practically, we had problems. We plan to avoid our artefact mitigation solution in the future work by a better image representation and by an explicit model for the CCD structure.

3. EXPERIMENTS

The principal goal of the experiments is to assess the quality of the detection certificate. We consider both kinds of errors: False detections (false positives) and missed streak images (false negatives). To capture the failure rate consistently, we use ROC analysis. A good overall performance characterization is the area under the ROC curve (AUC). It corresponds to the probability that a randomly chosen positive image instance will rank higher than a randomly chosen negative one [2]. Higher value is better, an ideal certificate would achieve $\mathrm{AUC} = 1$.

AUC depends on the difficulty of the detection problem instance. We therefore run a randomized experiment with simulated streaks of varying length, orientation, position, and amplitude. We expected that streak length and streak amplitude are factors that influence the detection problem difficulty. In order to make the experiment more realistic we used real streakless images as background.

3.1. Background Images

Images were obtained from 50cm TAOS sensor from Lulin observatory, Taiwan. This is the same data set used in [18]. The field of view of the telescope was $1.3^\circ \times 1.3^\circ$, the effective image size 2049(V)×2047(H), 16 bit monochromatic, 5.9 s exposure time. The telescope is passive (no sidereal tracking but regular repositioning to the initial inertial point). In total, there are 1986 images in the dataset obtained from seven-hour observations from three consecutive nights. Images contain artifacts of varying degree of severity, mostly reflections off clouds and stray light getting in the optical system. From this dataset we manually selected 1528 streak-free images that had no strong artefacts. These represent ground truth streakless images in our experiments.

It should be noted that since it is virtually impossible to eliminate every image containing a streak, the ground truth set of images is to some degree inaccurate.

3.2. Simulated Streak Images

The simulations are based on the aforementioned background set. A randomly generated additive streak with random amplitude is superimposed upon a randomly selected background image. The amplitude a of the generated streak is characterized by the signal-to-background ratio (SBR)

$$\mathrm{SBR} = 20 \log_{10} \frac{a}{\sigma}, \qquad [\mathrm{dB}] \tag{34}$$

where σ is the standard deviation of the background image values after excluding the upper half-percentile. In our data we typically had $\sigma = 51.4$ (median = 27.6, max = 201.6, min = 13.6).

The step-by-step simulation procedure is as follows:

- Select a random image from the set of background images (with replacement).
- Select a random $\mathrm{SBR} \in [-30,\, 20]\,\mathrm{dB}$ and determine streak amplitude a from (34).
- Generate random coordinates of a simulated streak.
- Render the streak in the image additively.

As a result, there were 1528 images in the streakless set and 5923 images in the streak set. This allows ROC analysis.

Fig. 1 shows an example of a simulated streak.

4. RESULTS AND DISCUSSION

Results are shown in Figs. 8 and 9.

Fig. 8 shows ROC curves for several classes of problem instance difficulty based on streak length $\Delta \in [10, 2680]\,\mathrm{px}$ and $\mathrm{SBR} \in [-20,\, 0]\,\mathrm{dB}$. The ROC value is obtained from all certification results in each of the listed sub-intervals. The ROC curve itself is obtained by varying the threshold T in (11).

Fig. 9 shows the AUC plots as a function of SBR. Each plotted point represents a subset of experiments for which the AUC is computed: The x-axis position is the average

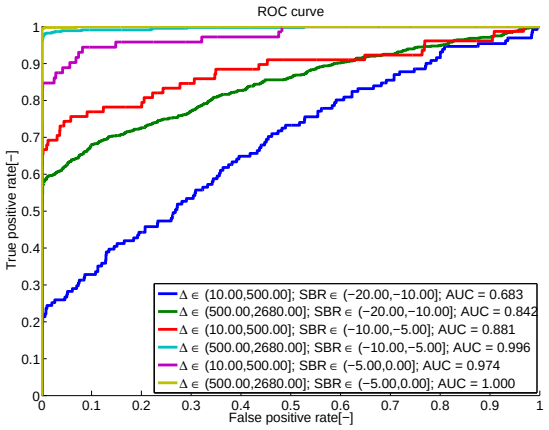

Figure 8. ROC curves for six classes of certification problem difficulty based on streak length Δ in pixels and SBR in dB.

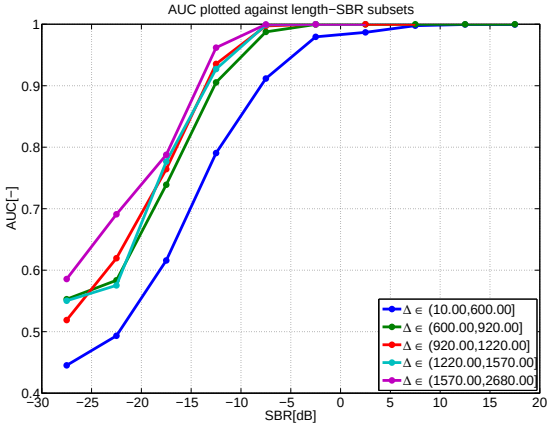

Figure 9. AUC curves as a function of certification problem difficulty. A high AUC value means a good overall assessment of the certification quality. Streak lengths Δ are in pixels.

value of the SBR per subset. This is done for several subsets of streak length, as specified in the legend.

We clearly see that the ability to certify a streak is decreasing with decreasing SBR and/or length of the streak. For instance, in the class of long streaks with good SBR (referenced last in the legend of Fig. 8, $\Delta > 500\,\mathrm{px}$ and $\mathrm{SBR} > -5\,\mathrm{dB}$, i.e. $0.56\,\sigma$) the certification is almost error-free. On the other hand, in the most difficult class of short streaks of low amplitude ($\Delta \in [10, 500]$ and $\mathrm{SBR} \in [-20, -10]\,\mathrm{dB}$) the certification is not very reliable with $\mathrm{AUC} = 0.683$, i.e. with almost 32% error rate. Since the streak images are modified background images, cf. Sec. 3.2), we consider the values of AUC close to 0.5 as indicating we are no longer able to distinguish between a streak image and a streakless image.

The AUC curves in Fig. 9 confirm the conclusions drawn from Fig. 8. It is interesting to note that except for the difficult class of short curves (blue, first in the legend), the performance is similar for the longer streaks, where the dominant success factor is streak SBR, not its length.

Our results seem to confirm and exceed results reported by other authors. For instance, [19] conclude: "[...] the streak significance per pixel about $0.6\,\sigma$, [...] is pretty challenging for typical objection detection techniques and invisible to the eye." For comparison, 0.6σ is about $\mathrm{SBR} = -4.4\,\mathrm{dB}$. An example of our simulation and detection at this level of SBR is shown in Fig. 10. As can be seen from the cyan ROC curve in Fig. 8, we can certify streaks with even lower SBR very reliably. If the streaks are shorter (red curve), we can still detect over 70 % of streaks, with false positive rate under 10 %.

We can see in Fig. 9 that streak lengths $\Delta \in (10, 600]$ are detectable with a greater error rate than the longer ones. Indeed, very short streaks or streak tracks detection require much higher SBR. For example, [5] claims "[to be capable] of extracting tracks of streak with signal-to-noise ratio near 1.5 (i.e. 3.5 dB)." They are forming longer streaks from such tracks, but the method is limited by the segment-then-track approach where the final performance is mostly determined by the segmentation; their result thus demonstrates the difficulty of detection of short streaks. Similarly, [12] works with very short streaks (10-pixel streaks) and signal intensities per pixel $1.0\,\sigma$ (0 dB). This we consider a very good result.

The work [11] reports detection probability for different length of streaks with the ratio between maximum pixel value and noise (MtN) of 0.6. This metric is not directly comparable to ours.

5. CONCLUSIONS

In summary, the proposed procedure shears the image over a well-chosen set of angles and performs vertical streak evidence integration per rotation. The shearing makes it somewhat similar to existing methods [12, 19]. Our method differs by avoiding exhaustive search over all angles, by unsupervised learning of parametric probability distributions per rotation angle for each input image, and by formulating the problem as MLBI which opens space to generalizations.

Although data and evaluation methodologies in our paper and the work of other authors are not identical, we can say our results confirm and partially exceed performance of the state-of-the art methods. In particular, in the class of difficult problem instances with SBR of $-5\,\mathrm{dB}$ to $0\,\mathrm{dB}$ and streak length 10 to 500 pixels, we achieved $\mathrm{AUC} \approx 0.97$, which means that the Bayesian detection certificate is wrong in just 3% of cases. Note that once the certificate confirms a streak presence, the MLBI procedure also detects it (it gives its position parameters).

In the current paper we considered only two statistical models: Streak is present/streak is absent in image. More models are possible: The k-th model would assume k streaks ($k \geq 0$). Almost arbitrary family of models is possible: Straight streaks vs curved streaks etc. Multiple level inference (MLBI) is quite a general principle. It can

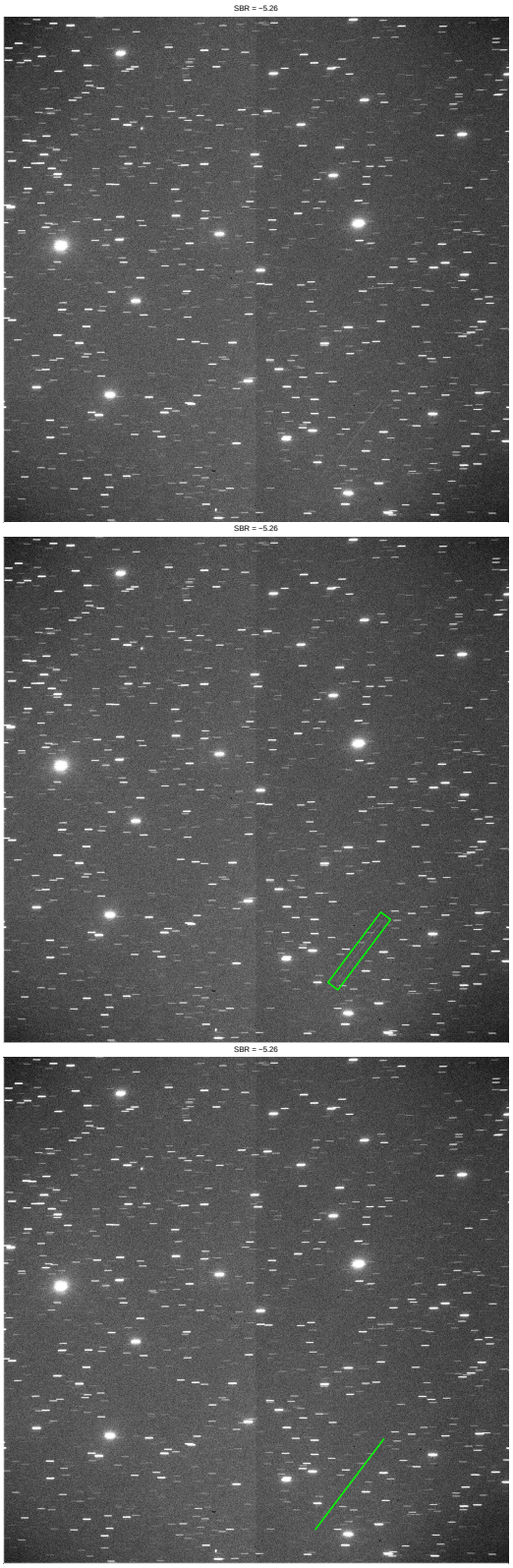

Figure 10. Example of a simulated streak with $\mathrm{SBR} = -5.26\,\mathrm{dB}$ *and length* $\Delta = 306\,\mathrm{px}$. *This shows that our simulation at a given SBR is consistent with the SNR of streak simulations used in [19]. From top to bottom: Simulated streak, streak with a frame indicating its pose, detection result.*

be thought of as an optimal procedure from information-theoretic point of view, a procedure that decides on the presence/detectability of an object in data.

For both p_0 and p_1, we assumed that the distributions are pixel-wise independent. This could be improved by considering dependencies among pixels, even in the streakless image model. One must not be too ambitious, though, because the polynomial computability of the evidences is easily lost.

ACKNOWLEDGMENTS

This work was supported by the CTU Internal grant SGS16/161/OHK3/2T/13. Special thanks go to Toshifumi Yanagisawa of JAXA who made their image data available to us.

REFERENCES

1. A. Ciurte and R. Danescu. Automatic detection of meo satellite streaks from single long exposure astronomic images. In *2014 International Conference on Computer Vision Theory and Applications (VISAPP)*, volume 1, pages 538–544, Jan. 2014.
2. T. Fawcett. An introduction to ROC analysis. *Pattern Recognition Letters*, 27(8):861 – 874, 2006.
3. M. Felsberg and G. Sommer. The monogenic signal. *IEEE Transactions on Signal Processing*, 49 (12):3136–3144, Dec. 2001.
4. P. S. Gural, J. A. Larsen, and A. E. Gleason. Matched filter processing for asteroid detection. *The Astronomical Journal*, 130(4):1951, 2005.
5. A. E. Kolessa. Detection of Faint Space Debris Elements with Unknown Orbits. In *6th European Conference on Space Debris*, volume 723 of *ESA Special Publication*, page 143, Aug. 2013.
6. J.-G. Leu. A computer vision process to detect and track space debris using ground-based optical telephoto images. In *Proceedings 11th IAPR International Conference on Pattern Recognition*, pages 522–525, Aug. 1992.
7. R. Litman, S. Korman, A. Bronstein, and S. Avidan. Inverting RANSAC: Global model detection via inlier rate estimation. In *Proceedings of the IEEE Conference on Computer Vision and Pattern Recognition*, pages 5243–5251, 2015.
8. D. J. C. MacKay. *Information Theory, Inference, and Learning Algorithms*. Cambridge University Press, 2003.
9. S. Maksim. A Comparison Between a Nonlinear, Poisson-based Statistical Detector and a Linear, Gaussian Statistical Detector for Detecting Dim Satellites. In *Advanced Maui Optical and Space Surveillance Technologies Conference*, page 44, Sept. 2012.

10. R. Marchant and P. Jackway. Feature detection from the maximal response to a spherical quadrature filter set. In *Proceedings International Conference on Digital Image Computing Techniques and Applications (DICTA)*, pages 1–8, Dec. 2012.

11. T. Schildknecht, K. Schild, and A. Vannanti. Streak Detection Algorithm for Space Debris Detection on Optical Images. In *Advanced Maui Optical and Space Surveillance Technologies Conference*, page 36, 2015.

12. M. Tagawa, T. Yanagisawa, H. Kurosaki, H. Oda, and T. Hanada. Orbital objects detection algorithm using faint streaks. *Advances in Space Research*, 57 (4):929 – 937, 2016.

13. M. Uetsuhara and N. Ikoma. Faint Debris Detection by Particle Based Track-Before-Detect Method. In *Advanced Maui Optical and Space Surveillance Technologies Conference*, Sept. 2014.

14. J. Virtanen, J. Poikonen, T. Säntti, T. Komulainen, J. Torppa, M. Granvik, K. Muinonen, H. Pentikäinen, J. Martikainen, J. Näränen, J. Lehti, and T. Flohrer. Streak detection and analysis pipeline for space-debris optical images. *Advances in Space Research*, 57(8):1607 – 1623, 2016.

15. L. Wietzke and G. Sommer. The signal multi-vector. *Journal of Mathematical Imaging and Vision*, 37(2): 132–150, June 2010.

16. T. Yanagisawa and A. Nakajima. Detection of small LEO debris with line detection method. *Transactions of the Japan Society for Aeronautical and Space Sciences*, 47(158):240–248, 2005.

17. T. Yanagisawa, H. Kurosaki, and A. Nakajima. The stacking method: The technique to detect small size of GEO debris and asteroids. Technical report, Japan Aerospace Exploration Agency (JAXA), 2008.

18. T. Yanagisawa, H. Kurosaki, H. Banno, Y. Kitazawa, M. Uetsuhara, and T. Hanada. Comparison between four detection algorithms for GEO objects. In *Proceedings of the Advanced Maui Optical and Space Surveillance Technologies Conference*, 2012.

19. P. C. Zimmer, M. R. Ackermann, and J. T. McGraw. GPU-accelerated faint streak detection for uncued surveillance of LEO. In *Proceedings of the 2013 AMOS Technical Conference*, 2013.